INSTITUTE OF PHYSICS PUBLISHING JOURNAL OF PHYSICS B: ATOMIC, MOLECULAR AND OPTICAL PHYSICS

J. Phys. B: At. Mol. Opt. Phys. **36** (2003) 499–510 PII: S0953-4075(03)54365-6

Laser-cooled ion plasmas in Penning traps*

J J Bollinger[1,4], J M Kriesel[1,5], T B Mitchell[2], L B King[1,6], M J Jensen[1], W M Itano[1] and D H E Dubin[3]

[1] Time and Frequency Division, National Institute of Standards and Technology, Boulder, CO 80305, USA
[2] Department of Physics and Astronomy, University of Delaware, Newark, DE 19716, USA
[3] Department of Physics, University of California at San Diego, La Jolla, CA 92093, USA

E-mail: john.bollinger@nist.gov

Received 30 September 2002, in final form 31 October 2002
Published 23 January 2003
Online at stacks.iop.org/JPhysB/36/499

Abstract

A laser-cooled ion plasma in a Penning trap provides a rigorous realization of a strongly coupled one-component plasma. After a brief review of the crystal structures that have been observed in Penning traps, we summarize two recent experiments. First we describe careful measurements of the stability of the plasma rotation which is controlled by a rotating electric field. We then discuss the excitation of plasma wakes produced by radiation pressure from a laser.

1. Crystalline structures in one-component plasmas

A one-component plasma (OCP) consists of a single species of charge immersed in a neutralizing background. The thermodynamic state of an OCP is determined by a single dimensionless parameter Γ known as the coupling of the plasma, where Γ is defined by

$$\Gamma \equiv \frac{1}{4\pi\epsilon_o}\frac{e^2}{a_{WS}k_BT}. \tag{1}$$

Here, ϵ_0 is the permittivity of the vacuum, e is the charge of an ion, k_B is Boltzmann's constant, T is the temperature, and a_{WS} is the Wigner–Seitz radius, defined by $4\pi(a_{WS})^3/3 = 1/n_0$, where n_0 is the ion density. Γ is simply a measure of the potential energy between nearest-neighbour ions divided by the ion thermal energy. Theoretical calculations for an infinite (or bulk) OCP predict that a liquid–solid phase transition to a body-centred cubic (bcc) lattice should take

* Contribution of the National Institute of Standards and Technology, an agency of the US government. Not subject to US copyright.
[4] Author to whom any correspondence should be addressed.
[5] Current address: Opto-Knowledge Systems, Torrance, CA 90503, USA.
[6] Current address: Department of Mechanical Engineering, Michigan Technological University, Houghton, MI 49931, USA.

place at $\Gamma \sim 172$ [1, 2]. OCPs are thought to exist in dense astrophysical objects [3]. An example is the outer crust of a neutron star, where the OCP consists of iron nuclei that move about in a degenerate background of electrons with an extremely high Fermi energy. The coupling in this system is thought to be in the range of 10–10^3.

Because the thermodynamic state of an OCP depends only on the dimensionless parameter Γ, OCPs of low density can exist, but only at low temperatures. Trapped ions provide a good, low-temperature realization of a strongly coupled OCP in the laboratory. Typical densities $>10^8$ cm^{-3} and temperatures $\lesssim$5 mK result in couplings $\Gamma \gtrsim 300$. In ion traps the trapping fields provide the neutralizing background. In fact, Malmberg and O'Neil [4] have shown this equivalence to be rigorously true in the Penning trap. Specifically, in thermal equilibrium the static thermodynamic properties of a laser-cooled ion plasma in a Penning trap are identical to those of a strongly coupled OCP of the same size (and shape). Because Penning traps use static fields for confinement, laser-cooling large numbers of ions ($>10^6$) is routine. Laser-cooled ions in a Penning trap therefore provide an exact laboratory realization of a strongly coupled OCP that may be large enough to exhibit bulk properties.

How many ions are required to form a bcc lattice, the predicted structure for an infinite OCP? This is a complicated question that depends on the shape and temperature of the plasma. Consider, for the moment, spherically shaped plasmas. (In a Penning trap both the trap voltage as well as the plasma rotation frequency can be used to set the shape of the plasma. See the next two sections.) For small spherical plasmas consisting of a few thousand ions, concentric shell structures are observed in both experiments [5] and simulations [6, 7]. The shells are sharp near the plasma boundary and consist of a two-dimensional hexagonal lattice that is distorted due to the conformation of the lattice to a spherical surface. Recent calculations by Totsuji *et al* [8] indicate that a bcc lattice appears to be the zero-temperature minimum-energy structure for a spherical OCP with $N \gtrsim 10^4$, where N is the number of trapped ions. Experimentally, Bragg scattering [9, 10] as well as imaging [11] of the ion fluorescence have been used, and bcc lattices exclusively observed in approximately spherical plasmas with $N \gtrsim 2 \times 10^5$. The preferred structures with $10^4 < N < 2 \times 10^5$ have not been experimentally investigated in a systematic way. However, we have observed other structures (such as fcc and hcp) in addition to bcc in this range. The observation of lattice types other than bcc in this number range may be due to finite temperature or perhaps some unrecognized perturbation. It is interesting to note that bcc lattices have been observed in Penning traps, but not rf (or Paul) traps. For example, a careful investigation of a spherically shaped, laser-cooled plasma of 40 000 $^{40}Ca^+$ ions was unable to observe any crystalline structure in the plasma interior [12]. In general, laser-cooling large numbers of ions in an rf trap requires more care than in the Penning trap.

In addition to spherically shaped plasmas, we have also studied the crystal structures formed in planar plasmas in a Penning trap [13]. Here the observed structure depends sensitively on the thickness and density of the plasma. For example, if the number of ions is not too great ($\lesssim$ a few thousand), the plasma rotation frequency can be lowered to where the ions form a single plane, perpendicular to the rotation (and magnetic field) axis. In this case a two-dimensional hexagonal lattice is observed. As the plasma rotation frequency is increased, the ions are compressed radially. At some point it is energetically favourable for the ions to form two planes rather than one. When this occurs we observe two rhombic planes. With further increases in the plasma rotation frequency the rhombic planes undergo a structural phase transition to hexagonal planes. Eventually the system forms three rhombic planes and the pattern repeats. For $\lesssim$10 planes the experimentally observed lattice types and structural phase transitions agree well with theoretical calculations [13–15] for the minimum-energy structures of a zero-temperature OCP that is infinite in two dimensions and harmonically confined in the third dimension.

2. Stability of the plasma rotation

Recently there has been a great deal of interest in using a rotating electric field perturbation to control the global $\boldsymbol{E} \times \boldsymbol{B}$ rotation of plasmas in Penning traps [16–18]. For crystallized ion plasmas, phased-locked control of the plasma rotation has been demonstrated [18]. This has important implications for atomic clocks [19] and for quantum computation with trapped ions [20]. In this section we discuss the limits to phase-locked control due to the application of a small torque produced by the radiation pressure of a weak laser beam. On long timescales we observe a small constant creep of the crystal orientation relative to the frame of the rotating electric perturbation. On short timescales the creep occurs in sudden angular jumps or 'slips' of the crystal orientation spaced by intervals when the crystal orientation is phase-locked or 'stuck' relative to the rotating perturbation. Creep and stick–slip behaviour similar to that observed here is found in many different and diverse systems: familiar examples include earthquakes [21] and studies of friction between two surfaces [22, 23]. Many of these systems, including the study presented here, exhibit a power-law distribution of the slip amplitudes, which may be indicative of an underlying critical point [24, 25].

In this work [26] we store $\sim$15 000 $^9Be^+$ ions in the NIST cylindrical Penning trap. Figure 1(a) shows the experimental setup [13, 18]. The $^9Be^+$ ions were confined radially by a uniform magnetic field $B = 4.465$ T (cyclotron frequency $\Omega_c/2\pi = 7.608$ MHz) in the $\hat{z}$ direction and axially by an electrostatic potential of $V_0 = 500$ V. The trap potential is quadratic near the trap centre and given by $m\omega_z^2(z^2 - r^2/2)/(2e)$, where the axial frequency $\omega_z/2\pi = 565$ kHz for $^9Be^+$. Here r and z denote the cylindrical radius and axial coordinate. In a quadratic trap, cold ion plasmas are spheroidal in shape (i.e. an ellipse of revolution) described by an aspect ratio $\alpha \equiv Z_o/R_o$, where $2Z_o$ is the axial extent of the cloud at $r = 0$ and the equation $Z(r) = \pm\alpha\sqrt{R_o^2 - r^2}$ describes the boundary of the plasma [27, 28]. Due to the axial magnetic field and the radial components of the ion space charge and trap electric fields, the ion crystal rotates at a frequency ω_r about the trap symmetry ($\hat{z}$) axis. At low temperatures the ion density is determined by ω_r according to $n_o = 2\epsilon_o m\omega_r(\Omega_c - \omega_r)/e^2$. In addition to $^9Be^+$ ions, ions of greater mass ('heavy ions') such as BeH^+ and $BeOH^+$ are created by reactions with $^9Be^+$ ions and background neutral molecules. For the work discussed here, typically 20–50% of the plasma consisted of heavy impurity ions. These ions are sympathetically cooled to temperatures similar to that of the $^9Be^+$ ions and, due to the rotation, centrifugally separate to larger radii, where they crystallize.

We applied an electric field perturbation rotating about the $\hat{z}$ axis at a frequency ω_{rp} to control ω_r [18]. The rotating perturbation applies a torque on the radial boundary of the plasma by creating a small-amplitude travelling wave. (In our experiment the travelling wave is excited on the non-fluorescing heavy ions.) The torque due to this wave is then transferred to the plasma's interior through the strong inter-particle forces, which act to bring the plasma to the same rotation frequency as ω_{rp} [27]. We observe similar stick–slip motion with both dipolar and quadrupolar rotating fields. However, most measurements, including those we report here, were taken with a dipolar rotating field. The radial binding force of the trap is due to the Lorentz force produced by the plasma's rotation through the magnetic field. Therefore, changing ω_r changes the radial binding force of the trap and provides a sensitive way to adjust the plasma shape (or aspect ratio) and structural phase of the plasma. In this work, $\omega_r \approx \omega_{rp} = 2\pi \times 22.8$ kHz, which produced a disc-shaped plasma consisting of five axial planes and a bcc-like crystal structure in the plasma's centre [13]. Because $\omega_r \ll \Omega_c$, the ion motion in a direction perpendicular to the magnetic field is determined principally by $\boldsymbol{E} \times \boldsymbol{B}$ guiding-centre dynamics [7].

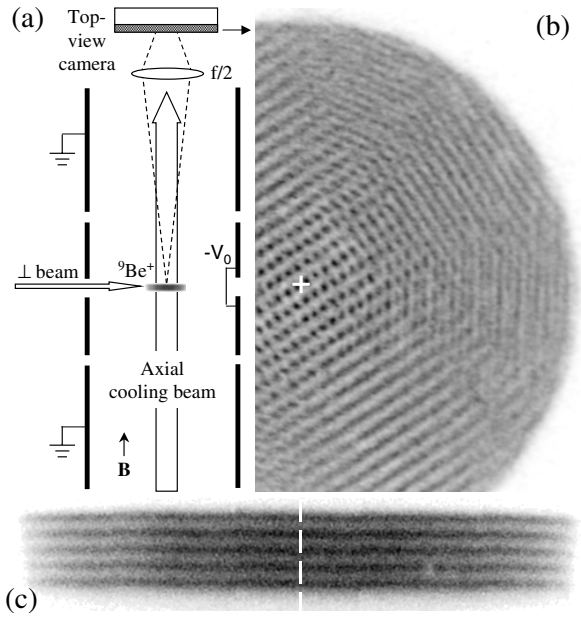

Figure 1. (a) Schematic illustration of the cylindrical Penning trap and the top-view imaging system. The side-view imaging system is not shown. (b) Strobed top-view image of a five-axial-plane $^9Be^+$ ion crystal with a bcc structure, similar to those used in this study. (c) Side-view image (unstrobed) of the same ion crystal. The diameter ($2r_{Be}$) of the $^9Be^+$ ions is 495 μm. Ions of greater mass are located at $r > r_{Be}$ but do not fluoresce in the laser beam. The rotation axis is indicated in (b) and (c).

The main cooling-laser beam ($\lambda = 313$ nm) was directed along the z axis. This beam was focused to a $\sim$0.5 mm waist at the ion crystal and had a power of $\sim$50 μW. A second cooling beam ($\perp$ beam in figure 1(a)), derived from the same laser, was directed perpendicularly to $\hat{z}$ and had a $\sim$70 μm waist and $\sim$1 μW power. Both the perpendicular and parallel cooling lasers were required to form a well defined crystal in the disc-shaped (or planar) plasmas discussed here. The $\perp$ beam is usually directed through the nominal radial centre ($r = 0$) of the crystal in order to minimize its applied torque while providing a low Doppler-cooling temperature [29]. In this experiment, though, we offset the $\perp$-beam position slightly (5–30 μm) from the plasma centre to produce a torque on the $^9Be^+$ ions in the same direction as the plasma rotation [30].

A series of lenses formed side- and top-view images of the ion fluorescence, with viewing directions respectively perpendicular and parallel to the magnetic field, on either an intensified charge-coupled-device (CCD) camera, or on an imaging photomultiplier tube. The resolution of the optical systems was $\sim$4 μm, while typical interparticle spacings were $\sim$15 μm. By detecting the ions' fluorescence synchronously with the rotating perturbation drive, images of the individual ions which make up the Coulomb crystals were obtained. Such an image is shown in figure 1(b) where the intensified CCD camera was used in the top-view position and strobed synchronously with the rotating perturbation drive. The image was accumulated over a 40 s period. The ion positions are well localized in the plasma centre; however, at larger radii they are blurred.

To investigate the blurring we used the imaging photomultiplier tube in the top-view position to record the positions and detection times of the fluorescence photons. Runs consisted of 125 ms intervals of data recorded each second over long periods of time (up to 5000 s).

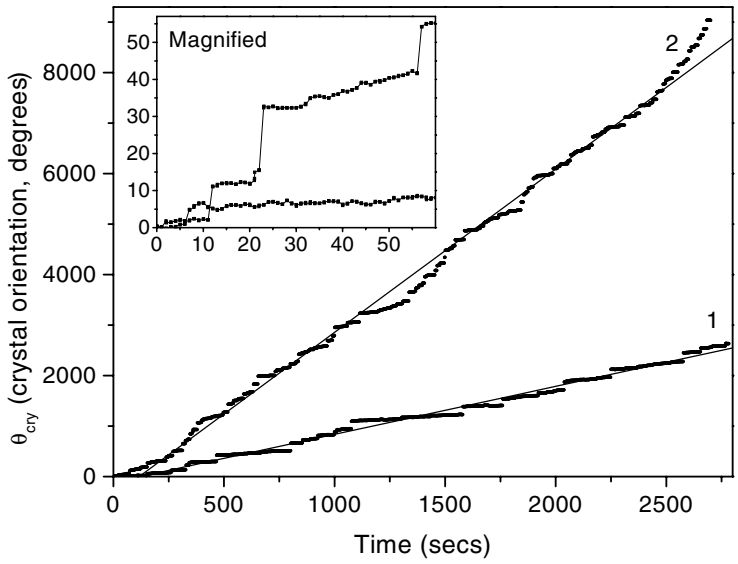

Figure 2. Crystal orientation θ_{cry} in the frame of the rotating perturbation for two data runs with different $\perp$-beam torques. The torque is greater in run 2. The lines are from a linear regression fit. The inset shows a magnified plot of the first 60 s of data.

Images similar to those in figure 1(b) were created for each 125 ms interval by constructing two-dimensional histograms of the ion fluorescence in the frame of the rotating perturbation. The orientation θ_{cry} of the central crystallized region in the rotating frame was determined (modulo π due to the bcc crystal's bilateral symmetry) with an uncertainty of $\sim 0.002\pi$ rad.

In figure 2 we plot $\theta_{cry}(t)$ for two runs that differ mainly in the amount of $\perp$-beam torque. Over long timescales the $\perp$-beam torque produces a slightly faster rotation (a rotational 'creep') of the $^9Be^+$ crystal relative to the rotating perturbation. For example, in run 2, $\Delta\omega \equiv \omega_r - \omega_{rp} \approx 2\pi \times 8$ mHz. Over shorter timescales, as shown in the figure 2 inset, much of this crystal rotation takes place with sudden jumps in θ_{cry}, 'slips', whose timescale is too fast to be captured by the top-view diagnostic. Let $\Delta\theta_{cry}$ denote the angular displacement between two successive measurements of θ_{cry}. The statistics of $\Delta\theta_{cry}$ consists of two components:

(1) a normal distribution (from measurement error) centred about zero with a width of $\sim 0.002\pi$, and
(2) a tail reaching out to large positive values that contains the infrequent large slips.

Due to the known sign of the $\perp$-beam torque and the π ambiguity mentioned above, we choose $\Delta\theta_{cry}$ to lie in the range $[0, \pi)$. To separate statistically significant slips from measurement error we further require $0.007\pi \leqslant \Delta\theta_{cry} \leqslant 0.97\pi$. We find that statistically significant slips account for greater than 90% of the measured change in θ_{cry}.

The $\perp$-beam torque is applied to all the $^9Be^+$ ions in the radial interior of the crystal. The rotating perturbation, however, applies its torque on the outer radial boundary of the heavy ions. We therefore believe the stress due to the competition between these torques is greatest in the region of the heavy ions and anticipate that the slips of figure 2 are due to ion motion between the radial boundary of the $^9Be^+$ ions, r_{Be}, and the overall radial boundary of the plasma. This is supported by the top-view images, which show most slips occurring as approximate rigid rotations of the $^9Be^+$ ions, and also by simulation work [26]. Because the slips occur at a

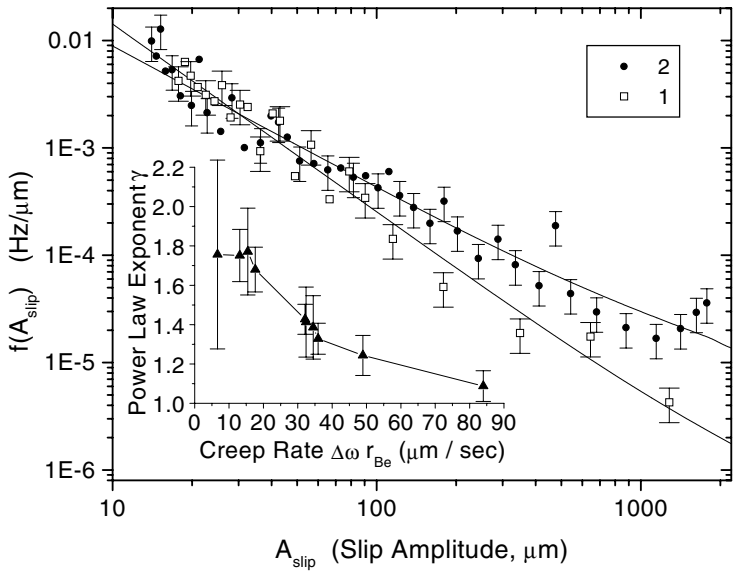

Figure 3. Distribution $f(A_{slip})$, where $f(A_{slip})\,\mathrm{d}A_{slip}$ is the frequency of slips between A_{slip} and $A_{slip} + \mathrm{d}A_{slip}$, for the two data runs shown in figure 2. The curves are fits to a power law with a cutoff as described in the text. The inset shows the measured power-law exponent γ versus applied torque, as parametrized by the creep rate, for all of the data runs.

radius greater than r_{Be}, and r_{Be} varied from run to run, we characterize a slip amplitude A_{slip} by the linear distance $\Delta\theta_{cry} r_{\mathrm{Be}}$.

Figure 3 shows the distribution $f(A_{slip})$ of slips for the two data runs shown in figure 2. The data were fitted to a power law [26], modified by the indistinguishability of slips that differ by $n\pi r_{\mathrm{Be}}$ where n is an integer. In the figure 3 inset we plot the measured power-law exponent γ as a function of the creep rate $\Delta\omega r_{\mathrm{Be}}$ for 10 data runs with the same rotating perturbation strength but different $\perp$-beam torques. We find that γ decreases as the creep rate, a measure of the applied $\perp$-beam torque, increases. Decreases in the stick–slip exponent with increased drive have been observed in many systems [23, 31, 32].

Most experiments exhibiting stick–slip behaviour are performed with 'constant-velocity driving' where the force is applied through an effective elastic coupling [23]. The driving force of the system is something like $F(t) = K(Vt - x(t))$, where 'x' is the 'position' of an element in the system (for example, the position of a bead or slider block in a chain), K is the effective spring constant coupling the applied force to each element in the system, and V is the constant average velocity that is imposed on the system. Stick–slip motion occurs for small V and K, and a critical point exists in the limit $V \to 0$ and $K \to 0$ [25, 31]. If a constant-velocity driving system gets stuck, it will eventually slip again because the driving force increases linearly until slip occurs. However, our experiment is performed under conditions more similar to 'constant-force driving' since the $\perp$-beam radiation-pressure force is constant in time and applied directly to the $^9\mathrm{Be}^+$ ions. Models of constant-force driving show a depinning transition at a critical force F_c and movement with constant average velocity proportional to $(F - F_c)^\beta$ for $F > F_c$ and critical exponent β [31].

Inspection of figure 2 shows that the time intervals between successive slips (the waiting periods) are typically many seconds. An analysis of the waiting periods shows an approximately Gaussian distribution with mean waiting periods ranging from 4 s for the highest $\perp$-beam torques to 12 s for the lowest $\perp$-beam torques. These waiting periods are

long compared to any known dynamical timescales due to internal modes of the system. In constant-force driving, if the system gets stuck for such a long period, it should permanently stick, which is not what we observe. One possibility is that the slips could be excited by a perturbation. By deliberately modulating the amplitude of the cooling and torquing lasers we have established that the amplitude noise present in these beams is not high enough to trigger slips. While determination of the exact cause of the slips will require further experimental work, molecular-dynamics simulations [26] indicate that the slips could be triggered by a rearrangement of a small number of heavy ions in the vicinity of a lattice defect. Possible causes of ion rearrangement include thermal fluctuations and collisions with neutral (room-temperature) background atoms. Once started, a slip eventually stops because the driving force of the $\perp$-beam is not sufficient to sustain continuous motion.

Minimizing the occurrence of the slips is important for some applications [19, 20]. Even without understanding their underlying cause, the slips can be minimized by minimizing the $\perp$-beam torque, either through active control of the $\perp$-beam position or by appropriate tailoring of the $\perp$-beam profile[7]. Increasing the strength of the rotating perturbation should also decrease the frequency of slips due to small ion rearrangements. Two runs taken with half the rotating perturbation strength of the data set analysed here showed an increase in the number of slips and rotational creep of the ion crystal.

3. Plasma wakes

Laser-cooled, spheroidal plasmas in Penning traps are a pedagogically interesting system for the study of plasma modes. This is because the modes can be calculated exactly [33, 34] and precise measurements of the mode eigenfrequencies [35] and eigenfunctions [36] are possible. In addition, mode studies have provided new experimental tools for probing and controlling plasmas of cold charged particles [37, 38]. Previous mode studies utilized electric fields acting on the entire plasma to excite *global* modes. In contrast, here [39] we excite *localized* waves by 'pushing' on a cold ion plasma with the radiation pressure of a focused laser beam. In this experiment, the ions rotate relative to the push beam, and the waves interfere 'downstream' to produce a stationary wake pattern, analogous to the wake behind a ship [40, 41]. The technique offers a new way to locally probe and diagnose cold ion plasmas and demonstrates a method for studying waves that were not accessible with previous techniques. In addition, wakes in Coulomb crystals are also a subject of current interest in their own right [42, 43], due primarily to recent experiments in which Mach cones and wakes were generated in two-dimensional (2D) dusty plasma crystals [44, 45].

The experimental setup is very similar to that described in the previous section. In the plasma wake experiment, the trapping potential was increased to $V_o = 1000$ V, leading to an axial frequency $\omega_z/2\pi = 800$ kHz. About 15 000–45 000 laser-cooled $^9Be^+$ ions were confined near the trap centre at a density of $n_0 \sim 2 \times 10^8$ cm^{-3}. We experimentally controlled ω_r with a dipolar rotating field perturbation [18, 46] as described in section 2. For the data presented here, the rotation frequency $\omega_r/2\pi$ ranges from 42.5 to 128 kHz with a respective range in aspect ratio of $\alpha = 0.005$ (corresponding to a two-dimensional single-plane disc of ions) to $\alpha = 1.0$ (corresponding to a thee-dimensional spherical ball of ions). For example, in figures 4(b) and (c) top- and side-view images are shown for a cloud with $\alpha = 0.042$ and $\omega_r/2\pi = 45$ kHz (for both images the radial extent of the cloud $R_o \approx 860$ μm is beyond the camera's field of view).

[7] The $\perp$-beam torque can be reduced with a beam that has a large waist and frequency dispersion across the waist that matches the ion Doppler shifts due to the plasma rotation.

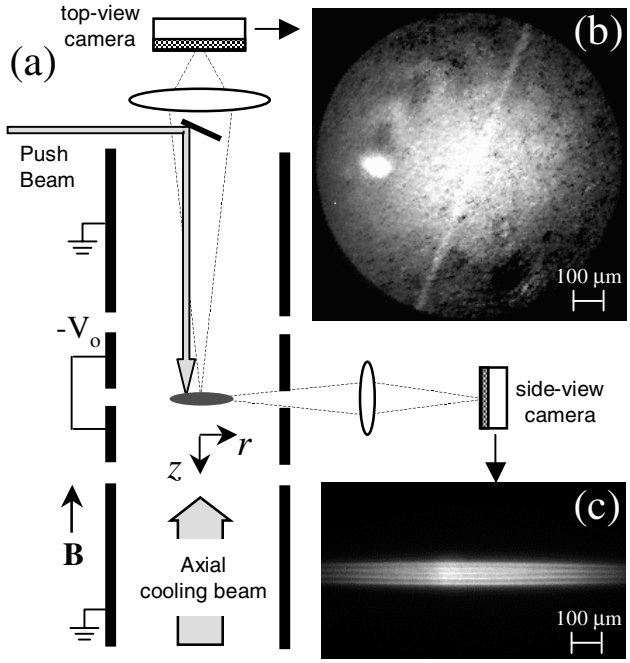

Figure 4. (a) Schematic illustration of the setup used to study wakes. (b) Top-view image of the fluorescence $I(r, \theta)$ from an $\alpha = 0.042$ Be^+ ion crystal. The white spot is due to the push beam and the diagonal white line is due to a perpendicular cooling beam (not shown in the schematic). (c) Side-view image of an $\alpha = 0.042$ crystal.

As discussed in the previous section, the main (axial) cooling beam has a 0.5 mm waist and is directed up along the trap axis; in addition, there is also a cooling beam directed perpendicularly to the trap axis (not shown in figure 4(a)). The push beam used to excite the waves is split off from the same 313 nm laser beam used for cooling, and is focused down to a relatively narrow waist of $w \approx 50$ μm. As shown in figure 4(a), this push beam is directed antiparallel to the axial cooling beam and is offset from the rotation axis by an amount R_{pb}, which we vary from 155 to 450 μm.

The ion fluorescence due to the axial cooling beam provides the primary diagnostic. Two sets of lenses form top- and side-view images of this fluorescence on either a CCD camera or an imaging photomultiplier tube. The wakes studied here are stationary in the lab frame, allowing us to simply collect the fluorescence continuously for about 30–120 s to generate an image. These images provide information about coherent ion motion since the relative intensity of an ion's fluorescence is highly sensitive to its axial velocity. In essence, we have a Doppler-velocimetry diagnostic: ions moving towards the red-detuned axial cooling beam (here defined to have velocity $v_z > 0$) encounter light that is Doppler-shifted closer to the resonance peak and hence fluoresce more strongly. Conversely, ions moving away from the beam ($v_z < 0$) fluoresce more weakly. For random thermal motion the variations in fluorescence average out; however, for coherent ion motion these variations enable the identification and measurement of waves and modes [36, 47].

Figure 5(a) is an example of Doppler velocimetry for a laser-induced wake. Here we use a greyscale to show the change in fluorescence due to the laser push $\Delta I(r, \theta) \equiv I(r, \theta) - I_o(r, \theta)$, where $I_o(r, \theta)$ is a 'background' image taken without the push beam and $I(r, \theta)$ is taken with the push beam (in this case figure 4(b)). The white spot in the left side of the image is due to the

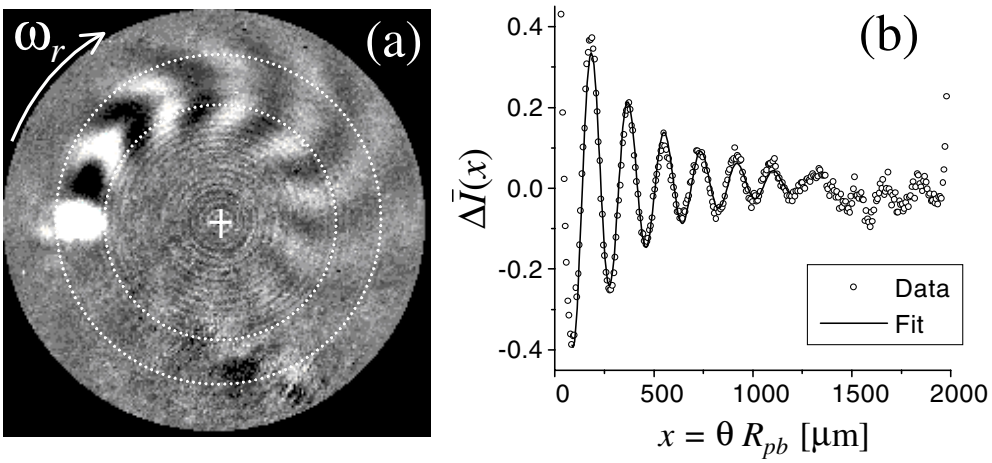

Figure 5. (a) Differential top-view image $\Delta I(r, \theta)$ of a laser-induced wake in a clockwise rotating Be^+ ion crystal. (b) Average fractional change in fluorescence $\Delta \bar{I}(x)$ for the annular region between the white circles in (a). Here, $x = 0$ is defined to be at the centre of the push beam. The solid curve is a fit to the data using a damped sinusoid (equation (3)).

additional scattered light from the push beam located at a distance $R_{pb} \approx 320\ \mu$m, whereas the downstream alternating dark and light arcs are variations in fluorescence due to coherent ion motion. We estimate that the change in fluorescence for the first peak of the wake corresponds to a change in velocity[8] of $\delta v_z \sim 1$ m s^{-1}. We further estimate that this δv_z corresponds to a maximum displacement[9] of $\delta z \sim 0.3\ \mu$m, which is much less than the interparticle spacing of $\sim 10\ \mu$m.

The laser-induced wakes observed here are analogous to the wake behind a ship moving in deep water [40, 41]. Due to the radiation pressure, ions receive a downward 'kick' as they rotate through the push beam, similar to the kick water experiences as a moving ship passes above. In both situations, the kick or push excites a large spectrum of waves with different wave numbers k and frequency ω, which travel in all possible directions. Wakes that are stationary in the frame of the source occur due to the constructive interference of waves that satisfy a stationary phase condition [40, 41]. The pattern of the wake depends upon the details of the appropriate dispersion relationship $\omega(k)$. The analysis of a wake is simplified directly behind the source along the direction of motion, where the stationary phase condition is satisfied by transverse[10] waves with a phase velocity ω/k that matches the relative velocity v of the source.

We thus obtain dispersion relationship data by analysing the wakes in an annular region directly behind the push beam to obtain a wavenumber $k = 2\pi/\lambda$, and then use the relationship $\omega/k = \omega_r R_{pb}$ to obtain a frequency ω. For example, figure 5(b) is a plot of the radially averaged fractional change in intensity

$$\Delta \bar{I}(x) \equiv \frac{\int r\, \mathrm{d}r\ \Delta I(r, x)}{\frac{1}{2\pi R_{pb}} \int \mathrm{d}x \int r\, \mathrm{d}r\ I_o(r, x)}, \tag{2}$$

where the radial integrals are performed over the annular region between the circles in

[8] Here we use the slope of the resonant transition curve at a detuning of 10 MHz.

[9] Here we use $\delta z = \delta v_z/\omega$ with $\omega/(2\pi) = 490$ kHz, where the method for obtaining this value of ω is described later in the text.

[10] In this context 'transverse' means that the wavefronts are approximately perpendicular to the direction of motion, in contrast to 'lateral' where the wavefronts are approximately parallel to the direction of motion.

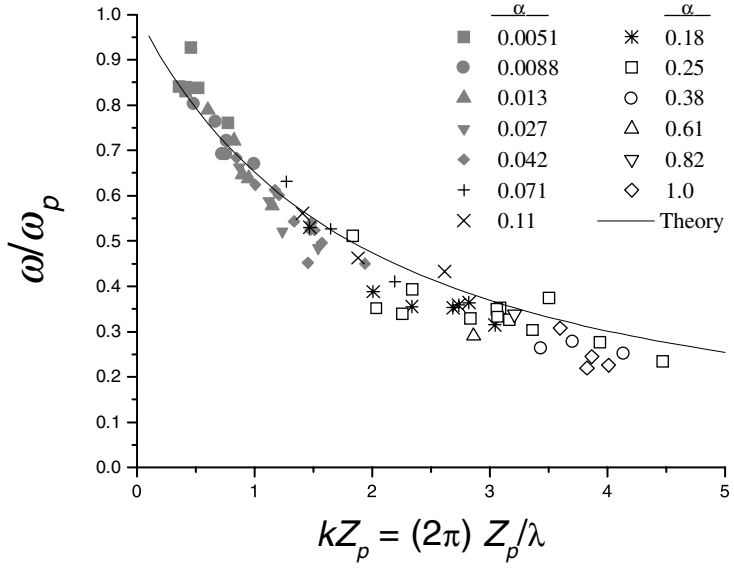

Figure 6. Measured dispersion relationship for various aspect ratios compared to a theoretical dispersion relationship for drum-head oscillations on an infinite planar slab of cold magnetized ions with thickness $2Z_p$.

figure 5(a), and $x \equiv R_{pb}\theta$ is the rotational distance from the centre of the push beam. As shown by the solid curve in figure 5(b), the oscillating wake is well fit by an exponentially damped sinusoid of the form

$$\Delta\bar{I}(x) = C_o + C_1 \sin(C_2 x + C_3)\mathrm{e}^{-C_4(x/\omega_r R_{pb})}. \tag{3}$$

Here, the C are fit coefficients where the wavenumber is $k \equiv C_2$ and the damping rate is $\gamma \equiv C_4$. (In the current experiments the damping is due to the axial cooling beam.) From the fit in figure 5(b) we get $\lambda = 2\pi/k = 185\ \mu$m, which in turn gives $\omega/2\pi = 490$ kHz using the calculated relative velocity of $v = \omega_r R_{pb} = 90$ m s^{-1}.

Dispersion relationship data obtained in this manner are shown in figure 6, where the different symbols correspond to different aspect ratios. Here the wave frequency ω is scaled by the plasma frequency $\omega_p = [2\omega_r(\Omega_c - \omega_r)]^{1/2}$ [27] (where $\Omega_c/2\pi = 7.6$ MHz is the bare cyclotron frequency); and the wavenumber k is multiplied by half the cloud thickness at the radial position of the push beam $Z_p \equiv \alpha\sqrt{R_o^2 - R_{pb}^2}$. For a single aspect ratio, different wake patterns were generated by changing R_{pb}, which effectively changed the relative velocity v of the push beam. Also shown in figure 6 is a theoretical dispersion curve. This is the dispersion curve for drum-head-like oscillations in an infinite, planar slab (i.e. $\alpha = 0$) of a cold, magnetized ion plasma [39]. The theoretical dispersion relationship agrees very well with the data. While the agreement with this slab model at low aspect ratio is better, as expected, the reasonably good agreement at higher aspect ratio ($\alpha \sim 1$) is somewhat surprising. This latter agreement indicates that the waves are excited locally and depend essentially upon the local plasma thickness Z_p with little dependence on the global shape of the plasma.

A theoretical description of the complete wake pattern must account for the nonzero size of the laser beam and the rotation of the plasma, and consider the complete set of oscillations with particle motion perpendicular to the plane of the slab (that is, not just the drum-head

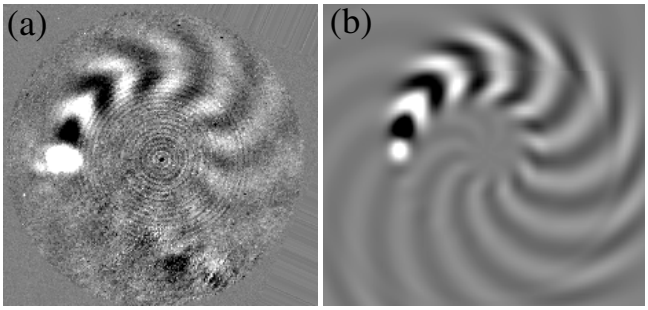

Figure 7. Scaled experimental image (a) of a wake for a plasma with $\alpha = 0.042$ shown alongside the corresponding theoretical calculation (b). The greyscale describes relative variations in the axial velocity of the ions.

oscillations). This is discussed in more detail in [39]. In figure 7 an experimental image $\Delta I(r, \theta)$ is shown and compared with the corresponding theoretical calculation. As in figure 5, we use a greyscale to represent the variations in axial velocity $\langle \delta v_z \rangle$, and scale each image by the value at the first peak of the wake. (In the experimental image, the extra fluorescence due to direct scattering of the push beam gives rise to the large white spot.) The experimental image in figure 7(a) is the same as that shown in figure 5(a), where the cloud is relatively thin ($\alpha = 0.042$) with $w = 50$ μm, $R_{pb} = 320$ μm, $\omega_r/2\pi = 45$ kHz, $\omega_p/2\pi = 825$ kHz and $Z_p = 33.5$ μm. The theoretical calculation shown in (b) used the above experimental values with $\gamma = 2.3 \times 10^5$ s^{-1}, which was determined from the damped sinusoid fit shown in figure 5(b). With no free parameters, the theoretical image is able to capture the qualitative features of the experimental image very well. For example, both images are dominated by arc-like transverse wakes; in addition, subtle features due to lateral wakes (see footnote 10), such as the line that appears to split the transverse arcs, appear in both the theoretical and experimental images.

The experiment described here demonstrates a method of exciting and studying a new class of waves in cold ion plasmas with potentially interesting applications. For example, the method can be used as a local probe of the plasma, providing information about such things as the local plasma thickness. In addition, with a more focused push beam than that used here, it may be possible to excite waves with wavelengths on the order of the interparticle spacing. Furthermore, with a slightly different setup, it may be possible to excite particle motion parallel to the plane of the slab (rather than perpendicular to it). For example, it would be interesting to excite (as yet unobserved) torsional $\boldsymbol{E} \times \boldsymbol{B}$ shear modes [48]. The restoring force in these modes is due only to the ion correlations and therefore shear modes are a sensitive probe of the correlations. Shear modes are also the lowest-frequency modes of ion plasmas in Penning traps. Because low-frequency modes can create difficulties in schemes which use trapped ions for quantum information, it is important to know the frequencies and level of excitation of these modes.

Acknowledgments

This research was supported by the US Office of Naval Research and the National Science Foundation (DHED). We thank Rich Fox, Carol Tanner, and David Smith for their comments on the manuscript.

References

[1] Ichimaru S, Iyetomi H and Tanaka S 1987 *Phys. Rep.* **149** 91
[2] Dubin D H E 1990 *Phys. Rev.* A **42** 4972
[3] Van Horn H M 1991 *Science* **252** 384
[4] Malmberg J H and O'Neil T M 1977 *Phys. Rev. Lett.* **39** 1333
[5] Gilbert S L, Bollinger J J and Wineland D J 1988 *Phys. Rev. Lett.* **60** 2022
[6] Rahman A and Schiffer J P 1986 *Phys. Rev. Lett.* **57** 1133
[7] Dubin D H E and O'Neil T M 1988 *Phys. Rev. Lett.* **60** 511
[8] Totsuji H, Kishimoto T, Totsuji C and Tsuruta K 2002 *Phys. Rev. Lett.* **88** 125002
[9] Tan J N, Bollinger J J, Jelenković B and Wineland D J 1995 *Phys. Rev. Lett.* **75** 4198
[10] Itano W M, Bollinger J J, Tan J N, Jelenković B, Huang X-P and Wineland D J 1998 *Science* **279** 686
[11] Bollinger J J, Mitchell T B, Huang X-P, Itano W M, Tan J N, Jelenkovic B M and Wineland D J 2000 *Phys. Plasmas* **7** 7
[12] Hornekær L and Drewsen M 2002 *Phys. Rev.* A **66** 013412
[13] Mitchell T B, Bollinger J J, Dubin D H E, Huang X-P, Itano W M and Baughman R H 1998 *Science* **282** 1290
[14] Schiffer J P 1993 *Phys. Rev. Lett.* **70** 818
[15] Dubin D H E 1993 *Phys. Rev. Lett.* **71** 2753
[16] Greaves R G and Surko C M 2000 *Phys. Rev. Lett.* **85** 1883
[17] Hollmann E M, Anderegg F and Driscoll C F 2000 *Phys. Plasmas* **7** 2776
[18] Huang X-P, Bollinger J J, Mitchell T B and Itano W M 1998 *Phys. Plasmas* **5** 1656
[19] Tan J N, Bollinger J J and Wineland D J 1995 *IEEE Trans. Instrum. Meas.* **44** 144
[20] Cirac J I and Zoller P 1995 *Phys. Rev. Lett.* **74** 4091
[21] Olami Z, Feder H J S and Christensen K 1992 *Phys. Rev. Lett.* **68** 1244
[22] Demirel A L and Granick S 1996 *Phys. Rev. Lett.* **77** 4330
[23] Ciliberto S and Laroche C 1994 *J. Physique* I **4** 223
[24] Bak P, Tang C and Wiesenfeld K 1987 *Phys. Rev. Lett.* **59** 381
[25] Vespignani A and Zapperi S 1998 *Phys. Rev.* E **57** 6345
[26] Mitchell T B, Bollinger J J, Itano W M and Dubin D H E 2001 *Phys. Rev. Lett.* **87** 183001
[27] Dubin D H E and O'Neil T M 1999 *Rev. Mod. Phys.* **71** 87
[28] Brewer L R, Prestage J D, Bollinger J J, Itano W M, Larson D J and Wineland D J 1988 *Phys. Rev.* A **38** 859
[29] Itano W M, Brewer L R, Larson D J and Wineland D J 1988 *Phys. Rev.* A **38** 5698
[30] Wineland D J, Bollinger J J, Itano W M and Prestage J D 1985 *J. Opt. Soc. Am.* B **2** 1721
[31] Lacombe F, Zapperi S and Hermann H J 2001 *Phys. Rev.* B **63** 104104
[32] Zapperi S, Cizeau P, Durin G and Stanley H E 1998 *Phys. Rev.* B **58** 6353
[33] Dubin D H E 1991 *Phys. Rev. Lett.* **66** 2076
[34] Bollinger J J, Heinzen D J, Moore F L, Itano W M, Wineland D J and Dubin D H E 1993 *Phys. Rev.* A **48** 525
[35] Heinzen D J, Bollinger J J, Moore F L, Itano W M and Wineland D J 1991 *Phys. Rev. Lett.* **66** 2080
[36] Mitchell T B, Bollinger J J, Huang X-P and Itano W M 1998 *Opt. Express* **2** 314
[37] Tinkle M D, Greaves R G, Surko C M, Spencer R L and Mason G W 1994 *Phys. Rev. Lett.* **72** 352
[38] Mitchell T B, Bollinger J J, Huang X-P and Itano W M 1999 *Trapped Charged Particles and Fundamental Physics* ed D H E Dubin and D Schneider (New York: American Institute of Physics) pp 309–18
[39] Kriesel J M, Bollinger J J, Mitchell T B, King L B and Dubin D H E 2002 *Phys. Rev. Lett.* **88** 125003
[40] Lord Kelvin (Sir W Thompson) 1887 *Proc. R. Soc.* **42** 80
[41] Faber T E 1995 *Fluid Dynamics for Physicists* (Cambridge: Cambridge University Press)
[42] Dubin D H E 2000 *Phys. Plasmas* **7** 3895
[43] Wang X, Bhattacharjee A and Hu S 2001 *Phys. Rev. Lett.* **86** 2569
[44] Samsonov D, Goree J, Ma Z, Bhattacharjee A, Thomas H M and Morfill G E 1999 *Phys. Rev. Lett.* **83** 3649
[45] Melzer A, Nunomura S, Samsonov D and Goree J 2000 *Phys. Rev.* E **62** 4162
[46] Huang X-P, Bollinger J J, Mitchell T B and Itano W M 1998 *Phys. Rev. Lett.* **80** 73
[47] Mitchell T B, Bollinger J J, Itano W M, Kriesel J M and Dubin D H E 2002 *IEEE Trans. Plasma Sci.* **30** 20
[48] Dubin D H E and Schiffer J P 1996 *Phys. Rev.* E **53** 5249